Temperature thresholds for polar stratospheric ozone loss: Electronic supplement

K. Drdla (Katja.Drdla@nasa.gov)

NASA Ames Research Center, Moffett Field, CA

Rolf Müller (ro.mueller@fz-juelich.de)

Forschungszentrum Jülich (ICG-1), Jülich, Germany

Summary

In this electronic appendix we present further details about the calculations and parameterizations of the onset of chlorine activation discussed in the main paper. In particular, we describe in further detail the model calculations used to deduce the parametrization for T_{ACL} (equation 2 in the main paper) and discuss the impact on the conclusions of the main paper of chlorine deactivation, and of the NAT surface and growth calculations. The microphysical and chemical simulations with the IMPACT model are described including an analysis of chemical ozone loss. Finally, we discuss observations of NAT particle concentrations and surface areas.

S1. Materials and Methods

S1.1 Assumed Conditions

Unless otherwise stated, calculations were done for conditions of 475 K, 5 ppmv H_2O, 10 ppbv HNO_3, and 1 $\mu m^2 cm^{-3}$ aerosol surface area. These conditions are referred to as standard stratospheric conditions, and are representative of early-winter conditions at about 20 km. Altitudes near 20 km have been most intensively studied both because ozone loss maximizes in this region and also because several aircraft campaigns have provided detailed in situ measurements at this altitude. T_{NAT} is calculated from the equation provided by Hanson and Mauersberger ([1])

Aerosol surface area used as an input value in this paper, in particular as input for T_{ACL}, is the surface area under non-polar conditions; for model calculations, the aerosol surface area was initialized at 210 K. At colder temperatures, the actual surface area can be larger than the input value due to aerosol growth. These increases are fully incorporated into all model calculations, for both binary and ternary solutions. To approximate the real vertical gradient of sulfate aerosol surface area, Figures 3d and 4 use a surface area profile in which the surface area varies according to the air density (i.e., the surface area in units of μm^2/mg-air is fixed); in this profile, the surface area at 475 K remains 1 $\mu m^2 cm^{-3}$. The resulting profile is comparable to measured values at background conditions ([2]).

S1.2 Calculating Chlorine Reactivity (Chlorine Activation Rate)

The chlorine reactivity has been calculated from a model that determines the

particle surface areas and reaction probabilities for all relevant particle types, based upon specified input conditions that include temperature, pressure, HNO_3, H_2O, $ClONO_2$, and HCl. The calculated loss rates of both $ClONO_2$ and HCl due to reactions (R1)-(R3) are summed. The resulting total is divided by the concentration of $ClONO_2$ and HCl to provide the normalized chlorine reactivity shown in Figure 1. The normalization reduces the sensitivity to the assumed chlorine levels (1 ppbv for $ClONO_2$ and 2 ppbv for HCl).

For the "NAT, Original" reactivity, NAT is assumed to form immediately at T_{NAT}. The surface area is calculated assuming all excess HNO_3 condenses (i.e., NAT is at equilibrium) and a NAT concentration of 1 cm^{-3}. This yields a large surface area (~7 $\mu m^2 cm^{-3}$). The reaction probabilities on NAT are assumed to be constant, specifically 0.2 for (R1), 0.004 for (R2), and 0.1 for (R3) ([3]).

The "NAT, New γ" case assumes the same large surface area as "NAT, Original". The NAT reaction probabilities are calculated using the *Carslaw and Peter* ([4]) formulation of the relative humidity dependence.

The "NAT, Current" case assumes that the NAT surface area is 0.1 $\mu m^2 cm^{-3}$. In reality, a range of NAT surface areas are likely to be possible at any given temperature, dependent upon details of the temperature history (section S2.1). The assumed surface area of 0.1 $\mu m^2 cm^{-3}$ is consistent with a NAT concentration of 10^{-4} cm^{-3} after five days of continuous growth. The NAT reaction probabilities are the same as in the "NAT, New γ" case.

For the "Liquid" simulation, the aerosol composition was calculated using the parameterization of *Carslaw et al.* ([5]). The liquid reactivities used the *Shi et al.* ([6]) formulation. This provides the reactivity of binary H_2SO_4/H_2O aerosol only. To

calculate ternary aerosol reactivities, the reactivity was assumed to be the same as that for the binary aerosol that would form under the same conditions (i.e., with the same water activity). Therefore differences between binary and ternary reactivities are caused solely by surface area differences.

S1.3 T_{ACL}: Model Calculations and Parameterization

T_{ACL} has been defined as the temperature at which the chlorine reactivity equals 0.1 day^{-1}. This value was chosen as the threshold reactivity necessary for detectable chlorine activation (~10%) over time scales of a day. A one-day timescale is typical for synoptic scale analyses: analysis temperature fields and satellite measurements typically provide global coverage one or two times per day. 10% chlorine activation is equivalent in the current atmosphere to about 0.35 ppbv of ClO, which is a clearly recognizable enhancement relative to background levels of ~0.1 ppbv. Maps of ClO from satellite data have used thresholds of 0.3 and 0.45 ppbv to define regions with elevated ClO ([7]).

Since liquid reactivity varies continuously with temperature, T_{ACL} is not an absolute threshold, above which no activation occurs and below which activation is instantaneous. However, it does provide a useful diagnostic of where chlorine activation and ozone loss are most likely. In addition, for understanding how chlorine activation responds to changing conditions or varies from winter to another, relative changes in T_{ACL} are more important than the exact value. In this context, it is important to establish a constant definition that can be used under all conditions.

Model simulations confirm that 0.1 day^{-1} and T_{ACL} represent meaningful thresholds for polar ozone loss. Winterlong simulations of the 1999-2000 Arctic winter (described

in section S1.6) have been examined to determine the model conditions necessary for enhanced ozone loss. Figure S1 shows, for each individual model air parcel in the "FullPSC" simulation, a comparison of the total ozone loss with the coldest temperature to which the air parcel was exposed for one day. Exposure for one day was used instead of the instantaneous minimum temperature because activation does not occur instantaneously. Enhanced ozone loss is detectable starting in air parcels that have spent one day below T_{ACL}. Average ozone loss in the first temperature bin below T_{ACL} exceeds the average ozone loss above T_{ACL} by 1 σ.

Additional simulations ("LiqTACL") were done in which the model temperature histories were modified so that the temperature never dropped below T_{ACL}. The duration of exposure to temperatures at or below T_{ACL} is unchanged, but the aerosol reactivity is effectively capped at 0.1 day^{-1}. Even in this extreme case, the relative decreases in chlorine activation and ozone loss are only 18 to 40% (Table S1). The greatest change is in vortex-averaged Antarctic ozone loss, which is reduced from 86.9% to 50.3%. The ability to produce most of the ozone loss and chlorine activation without any exposure to temperatures below T_{ACL} demonstrates that the primary factor controlling chlorine activation is just the existence of temperatures at or below T_{ACL}. The details of what happens at temperatures below T_{ACL} have only a secondary role and can all be reproduced accurately with a model in which there is no PSC formation of any type.

Using a reactivity of 0.1 day^{-1} to define T_{ACL}, its value has been calculated for a wide range of stratospheric conditions, using the same aerosol chemistry model as in Figure 1 (section S1.2). The parameters that were varied were H_2O (range 1 to 20 ppmv), sulfate surface area (0.1 to 100 $\mu m^2 cm^{-3}$), potential temperature (375 to 700 K), and

HNO_3 (1 to 20 ppbv). Calculations assuming both a ternary and a binary liquid solution were done for each combination of H_2O, surface area, and potential temperature. All possible combinations of the parameters were examined; in all, T_{ACL} was calculated for more than 500,000 different conditions.

Across almost the full range of tested conditions, T_{ACL} occurs at temperatures warmer than the onset of STS, and therefore T_{ACL} shows no significant dependence upon HNO_3. The only conditions under which T_{ACL} was sensitive to HNO_3 were when both surface area and H_2O were small; even then the maximum change in T_{ACL} due to varying HNO_3 was 0.8 K. Otherwise, i.e., for all conditions with surface area greater than 0.25 $\mu m^2 cm^{-3}$ or H_2O greater than 3.5 ppmv, the maximum difference between T_{ACL} calculated assuming 10 ppbv HNO_3 and T_{ACL} for a binary solution was 0.40 K, with a root-mean-square difference of 0.09 K. For an increase from 10 ppbv HNO_3 to 20 ppbv HNO_3, the maximum difference was 0.38 K, rms difference 0.09 K. Furthermore, at T_{ACL} the average HNO_3 weight percent of the liquid aerosol is 0.8%; the surface area is on average 2% larger than the surface area at 210 K. Therefore, the full set of calculations support the conclusion that the onset of chlorine activation is caused by aerosol that is nearly indistinguishable in size from midlatitude stratospheric aerosol, and cannot be characterized as a polar stratospheric cloud; increases in surface area are not necessary for the chlorine reactivity to reach 0.1 day^{-1}.

The parameterization of T_{ACL} (equation 2) was developed from the model-calculated values using a least-squares fit. Two separate fits were created, to allow either potential temperature or pressure to be used as the vertical coordinate. Both fits match the data to comparable accuracy. For most conditions (potential temperature 400 to 620

K, surface area 0.2 to 15 $\mu m^2 cm^{-3}$, H_2O 2 to 16 ppmv), the difference between model and fit is less than 0.25 K. Over the full range of conditions, the rms difference between model and fit is 0.21 K.

Figure 4 is calculated from daily UK Met Office analysis temperatures, interpolated onto potential temperature surfaces. Both A_{ACL} and A_{NAT} assume 5 ppmv H_2O. For A_{NAT}, HNO_3 is initialized from a MkIV balloon profile ([8]) measured on December 3, 1999; denitrification is not incorporated into the calculation. For A_{ACL}, the "varying SA" sulfate surface area profile was used, similar to Figure 3d (see section S1.1).

S1.4 Chlorine Deactivation

This paper relies on the chlorine activation rate alone to establish where high chlorine levels and thus ozone loss are likely. The amount of active chlorine will be determined, however, by both the chlorine activation and deactivation rates. In general, a full photochemical model is necessary to properly quantify the extent of the chlorine activation and the resulting ozone loss. The approximations made in this analysis are possible because during polar winter chlorine deactivation rates are very slow. As long as there is relatively little solar illumination, T_{ACL} can be used to estimate regions with elevated chlorine.

The reactions that lead to chlorine deactivation are all initiated, directly or indirectly, by photolysis. HNO_3 photolysis, in particular, is the primary source of NO_2, which reacts with ClO to form $ClONO_2$ ([9]). This reaction requires UV radiation and therefore is not efficient at low solar elevations, although under the same conditions there can be enough longer wavelength illumination to allow ozone loss to occur.

Tests have been done using a full photochemical model to determine the conditions under which chlorine deactivation is too slow to compete with heterogeneous activation, assuming no denitrification. The criteria used were that the timescale for deactivation was more than 15 days (taking into account all possible chlorine deactivation pathways) and that the amount of available NO_x ($NO+NO_2$) was less than 0.5 ppbv (so that less than one-quarter of the chlorine budget could be rapidly deactivated by any existing NO_x). Under a range of stratospheric conditions, these conditions were always met by air parcels in which the solar elevation was at most 20° (or, equivalently when the minimum solar zenith angle is 70° or more). The solar elevation has been chosen as a convenient metric because it does not require any photochemical modeling.

In midwinter, the region where the solar elevation is at most 20° extends from 47° latitude to the pole. At 70° N, these conditions are present from September 30th to April 2nd; at 70°S, from April 1st to October 1st. In both hemispheres, these dates cover the periods of importance for polar chlorine activation. In the southern hemisphere, cold temperatures are possible approaching October 1st, but only under severely denitrified conditions. The denitrification is sufficient to suppress chlorine deactivation even in the presence of higher levels of sunlight.

Because the equations derived for T_{ACL} are only applicable during polar winter conditions, they cannot be used in regions such as the tropical stratosphere where similarly cold temperatures can occur. In the equatorial region, the greater solar exposure will cause any heterogeneously activated chlorine to be rapidly quenched by the fast gas-phase reactions. Therefore, similarly cold temperatures in the tropics may have little or no effect on ozone.

S1.5 NAT Surface Area and Growth Calculations

In Figure 2a, the maximum surface area is the equilibrium surface area determined from geometry alone without any microphysical modeling. All available HNO_3 (S_{NAT}=1) is assumed to condense onto the specified number of particles and all particles are assumed to be equally sized. Since the total NAT volume is fixed, the surface area ends up being proportional to $n^{1/3}$, where n is the concentration. The assumed conditions for all calculations in Figure 2 are 192 K (three Kelvin below T_{NAT}), 475 K, 10 ppbv total HNO_3, and 5 ppmv total H_2O.

The NAT growth rates in Figure 2b and the surface areas (other than the maximum surface area) were all determined using a microphysical model of PSCs ([10]). The model was initialized with the specified number of NAT particles, initial radii 0.1 μm. The temperature was kept constant at 192 K (T_{NAT}-3 K) for the entire simulation. The chosen temperature maximizes NAT growth rates (at colder temperatures, gas-phase HNO_3 is depleted by liquid phase HNO_3 uptake, inhibiting NAT growth); in the real atmosphere with varying temperatures, growth time scales could be even longer than those shown. Other parameters were also chosen to maximize particle growth, e.g., HNO_3 accommodation coefficient assumed to be unity. Particle altitudes were held fixed for the entire calculation. The denitrification timescale was calculated as the time necessary for 10% (1 ppbv) of the total HNO_3 to sediment 1 km. Since particles did not actually sediment in this simulation, the fall distance was instead calculated by integrating the model-determined fall velocities over the duration of the simulation.

Liquid particles were assumed to be simultaneously present in the microphysical

simulations, assuming a fixed total (liquid + NAT) particle concentration of 10 cm^{-3}; the mode radius of the liquid particles was 0.08 μm. At high NAT concentrations the slight decrease in liquid surface area reflects the decreased liquid particle concentration. The assumed conditions are too warm for formation of STS; at colder temperatures, STS formation will enhance the liquid surface area by a factor of ten.

S1.6 Microphysical Simulations of Winter Evolution

A model with full PSC microphysics, heterogeneous chemistry, and gas-phase chemistry has been used to provide confirmation of several aspects of this study. The IMPACT model was used to simulate both the 1999-2000 Arctic winter and the 2000 Antarctic winter. The simulations for the 1999-2000 Arctic winter use the same methodology as previous studies (*S10*, [11]). A comparable methodology was adopted for the Antarctic winter, where 3517 trajectories were simulated, extending from April 15th 2000 to November 15th 2000, ranging in potential temperature from 400 K to 750 K on July 15th. Table S1 summarizes the microphysical scenarios simulated for this study.

The "FullPSC" scenario was used to examine PSC characteristics in a simulation with complete microphysics. The microphysics are the same as the "HetFrzB" (0.02%) scenario which has been found to best match measurements in both the Arctic (*S10*) and Antarctic ([12]). The formation of a small ($<10^{-2}cm^{-3}$) concentration of NAT particles allows realistic denitrification to occur. The rest of the particles are liquid, with HNO_3 uptake to form STS PSCs at colder temperatures. In the Antarctic, significant dehydration is simulated as a result of widespread ice PSC formation.

Table S2 shows how much chlorine activation over the entire winter can be

attributed to each particle type. Binary liquid particles are responsible for the majority, but definitely not all, of the chlorine activation in both the Arctic and the Antarctic. Ice particles always play a small role: even in the Antarctic, where ice PSC formation was widespread, only 0.6% of the activation occurred on ice particles. For the other PSCs, this simulation alone cannot clarify whether the PSC particles were actually necessary for activation, or alternatively whether in replacing the aerosol, the PSCs also just replaced the chemistry that otherwise could have occurred on the aerosol.

The second scenario, "Liquid," was used to isolate the effects of denitrification and dehydration. This scenario included only liquid-phase particles (no NAT or ice PSCs), but ternary solution formation was allowed, so STS PSCs were prevalent. As discussed by Drdla and Schoeberl (*S11*), maximum chlorine activation is almost identical in the "Liquid" and "FullPSC" simulations. The differences in ozone loss (Table S1) can all be attributed to the effects of denitrification and dehydration.

The remaining scenarios further alter the "Liquid" scenario to examine the chlorine activation processes specifically. "LiqBin" has only binary solution liquid aerosol particles. Without any HNO_3 uptake, STS PSC formation is suppressed and the liquid particle surface area is not enhanced at cold temperatures. The reactivity corresponds to the "Liquid (binary)" calculation in Figure 1. Chlorine activation and ozone loss are nearly identical in "Liquid" and "LiqBin," clearly showing that the chlorine activation is not sensitive to the PSC characteristics or the surface area enhancements caused by the PSCs. Under the conditions where PSCs would normally form, reactivities on binary aerosol alone are fast enough to activate any available chlorine. PSC formation is not necessary for chlorine activation or for ozone loss.

In “LiqTACL” and “LiqTACL2,” the conditions along each simulated trajectory were artificially altered to further constrain the importance of PSC-type temperatures. For “LiqTACL,” the temperature was set to be equal to T_{ACL} during any period when normally the temperature would have been less than T_{ACL}. Temperatures were not altered at conditions above T_{ACL}. Similarly for “LiqTACL2,” the minimum temperature was set to be 2 K below T_{ACL}. These temperatures are warm enough that STS PSC formation is prevented from ever occurring, i.e., the liquid surface area never increases above background levels. In addition, the reactivity of the liquid aerosol is effectively capped: in “LiqTACL,” the reactivity never exceeds 0.1 day^{-1} and for “LiqTACL2" the maximum is roughly 0.3 day^{-1}. Chlorine activation and ozone loss are reduced in these simulations but even with these substantial perturbations to the chemistry, chlorine activation exceeds 50% and ozone loss remains significant.

Therefore, “LiqTACL” shows that exposure to temperatures at or below T_{ACL}, with reactivities no greater than 0.1 day^{-1}, is by itself responsible for most of the model's chlorine activation and ozone loss. Allowing binary liquid aerosol reactivity values greater than 0.1 day^{-1} (“LiqBin” simulation), as is normally predicted below T_{ACL} without any required changes in aerosol surface area, enhances the chlorine activation but only by 18-20%. Surface area increases, due to STS, NAT, or ice PSCs (“Liquid” and “FullPSC” simulations), are not necessary to account for any of the modeled chlorine activation. NAT and ice PSC formation only alter the model chemistry through denitrification and dehydration.

S2. Supporting Text

S2.1 NAT Particle Concentrations

The NAT particle concentrations in Figures1 and 2 are meant to be representative of the NAT PSCs that form during the early winter period, in particular during the first five to ten days below T_{ACL}. Within the first five days of exposure to temperatures below T_{ACL}, half of the chlorine can be activated. Therefore the processes during this early period of PSC formation are sufficient to cause most of the chlorine activation, and are more important in determining the overall extent of chlorine activation than processes at colder temperatures. Even though colder temperatures can lead to much larger chlorine reactivities (in particular when water ice PSCs are present), these faster reactivities cannot cause any chlorine activation if the reactants have already been depleted (*S11*). In most cases, complete reaction of $ClONO_2$ is possible on liquid aerosol before temperatures reach 4 K below T_{NAT}. Excess HCl may still be present, but cannot be activated without reaction partners.

The "NAT, Original" calculations adopt a NAT concentration of 1 cm^{-3}. While this value is representative of the NAT concentration in many models, the range of different approaches taken by models has led to varying values for the NAT concentration. Some early models assumed much higher values ([13], [14]), with NAT concentrations up to 15 cm^{-3} and NAT surface areas up to 25 $\mu m^2 cm^{-3}$. Many models initialize NAT particles using a fixed particle size instead of fixed concentration; 1 μm radius is typically assumed ([15]). For 10 ppbv HNO_3, the resultant NAT concentration is 0.4 cm^{-3}, with a surface area of 5 $\mu m^2 cm^{-3}$. In all these cases, the chlorine activation is comparable to the "NAT, Original"

calculation. In general, assuming a NAT concentration greater than 10^{-2} cm^{-3} (or NAT radii less than 2.5 μm) produces NAT surface areas larger than the sulfate aerosol surface area, and these large surface areas are possible in the first day after temperatures fall below T_{NAT} (Figure 2a).

However, observational evidence for NAT concentrations of ~1 cm^{-3} (or equivalently 1 μm NAT particles) is very limited. These concentrations originated from in situ observations of PSCs ([16], [17], [18], [19]), which provided particle size distributions with at best qualitative information on the presence of condensed phase HNO_3; the phase or composition of the particles was not measured. At the time the measurements were made, NAT was the only known HNO_3-containing condensed phase in the stratosphere, so all PSCs forming above the ice frost point were identified as NAT clouds.

Since then, the existence of liquid STS PSCs has been recognized ([20], [21], [22], [23]). In particular, a PSC event measured on January 24th 1989 provided decisive evidence for the existence of liquid-phase PSCs. However, these exact same measurements were used by earlier studies (*S13*, *S14*) to characterize NAT PSCs. Therefore "typical" NAT PSC concentrations of ~1 cm^{-3} were originally derived from measurements of liquid-phase PSCs that were mistakenly identified as NAT clouds.

Although a complete understanding of NAT particles and their microphysics remains elusive, the observational evidence increasingly demonstrates that NAT concentrations are very small, especially when air first cools to temperatures near T_{NAT}. Two independent observations have found that for large-scale (synoptic) conditions, the NAT particle characteristics are at most 10^{-3} cm^{-3} during the first five days that PSCs spend below T_{NAT}. One set of Arctic observations found NAT particle concentrations of

$1.6 \bullet 10^{-4}$ cm^{-3} in air that had been at temperatures between T_{NAT}-3 K and T_{NAT} for ~20 hours ([24]). In another set of observations, air that had been below T_{NAT} for one to five days contained NAT concentrations of ~10^{-3} cm^{-3} ([25]). These are comparable to the concentrations used in the "NAT, Current" scenario, demonstrating that during the initial stages of chlorine activation NAT surface areas are too small for NAT to control activation.

Even later in the winter, NAT concentrations remain small. The initial observations of "NAT rocks" (*S24*, [26]) demonstrated concentrations of 10^{-5} to 10^{-3} cm^{-3} over extensive geographical regions late in the Arctic winter. The large NAT particle sizes imply comparably small concentrations over most of the particle lifetime. To produce such large particles, days of continuous growth are necessary; a second population of numerous small NAT particles would effectively stop particle growth by rapidly removing all excess HNO_3 from the gas-phase. The failure to detect "NAT rocks" prior to 2000 does not imply that their occurrence is rare, only that these particles are difficult to measure. The optical counters that have been used to measure particle concentrations routinely detect only concentrations greater than 10^{-3} cm^{-3}; even with extended averaging, the lower limit is 10^{-4} cm^{-3} ([27]). Furthermore, in earlier cases with trace numbers of large particles, the particles were assumed to be ice (*S18*) in the absence of any particle composition measurements. Conclusive identification of "NAT rocks" required instrument characteristics that were not introduced until the 1999-2000 Arctic winter: detection specifically of the HNO_3 mass contained in individual large particles, with sensitivity to concentrations of 10^{-5} to 10^{-3} cm^{-3} (*S26*).

Remote observations are consistent with small NAT particle concentrations. Lidar

depolarization has been used for years to detect solid-phase PSCs; the term "Type 1a PSC" was introduced to describe the most common type of solid-phase PSC detected by lidar. A multiyear climatology of Antarctic lidar observations confirms that Type 1a PSCs are widespread and constitute the majority of PSC observations ([28]). Using a different detection technique, Type 1a PSCs were also found to be widespread in satellite extinction data ([29], [30]).

Particle concentration is not directly measured by lidar, and is particularly difficult to constrain for Type 1a PSCs. Lidar data can be analyzed to infer the particulate mass and, for smaller particles, the average radius. From those two quantities, the concentration can be inferred. A detailed analysis ([31]) found that the condensed mass in Type 1a PSCs was consistently small (less than 20% of the available HNO_3 had condensed) and that the particle radius was at or beyond the upper limit of the retrieval, 1 μm. Assuming 1 μm radius, Toon *et al.* concluded that the NAT concentration was less than 0.1 cm^{-3}. However, a larger radius, typical of NAT rocks, would be equally consistent with the lidar data. For 5 μm particles, the derived concentration from the same observations would be less than 10^{-3} cm^{-3}. The low mass is also consistent with a low concentration. As shown in Figure 2a, concentrations $<10^{-2}$ cm^{-3} are necessary to limit the NAT growth rate to the point where only 20% of the HNO_3 would condense in a day. Therefore lidar data of the most common type of NAT PSC shows that NAT concentrations are definitely less than 0.1 cm^{-3}, and potentially smaller than 10^{-3} cm^{-3}.

In contrast, lidar observations show clearly different characteristics for a small subset of NAT clouds, labeled "Type 1a enhanced" PSCs ([32], [33]). These clouds are primarily detected downwind of mountain-induced lee-wave clouds, where local

temperatures have been below the ice frost point. The distinctly larger backscatter from these clouds is produced by enhanced NAT particle concentrations, greater than 0.1 cm^{-3} ([34]). The existence of two qualitatively different classes of NAT PSCs requires substantial differences in the characteristics of the two types of clouds, reinforcing the conclusion that the NAT concentration of Type 1a PSCs is orders of magnitude smaller than in "Type 1a enhanced" PSCs. "Type 1a enhanced" PSCs are not frequently observed: over multiple years of observations, less than 10% of all observations can be identified as "Type 1a enhanced," even for an Antarctic site with frequent mesoscale temperature perturbations (*S28*). Furthermore, these high-concentration NAT clouds are specifically generated downwind of evaporating water ice clouds; they do not form under the conditions where chlorine activation first occurs, especially at the synoptic scale.

A single value cannot be expected to properly represent the NAT surface area under all conditions; more than one order of magnitude variability is likely. Until the microphysics controlling NAT particle formation is better understood, predictions of the NAT surface area for given conditions will be uncertain. The 0.1 $\mu m^2 cm^{-3}$ surface area used in the "NAT, Current" calculation is a value within the probable range of early winter surface areas. Lower values have been measured in a 20-hour-old PSCs (*S24*); higher values are possible given sufficient time (i.e., a NAT concentration of 10^{-3} cm^{-3} could result in a NAT surface area approaching 0.7 $\mu m^2 cm^{-3}$). The chlorine reactivity varies linearly with surface area, so the effect of any change to the assumed surface area can be easily estimated. From Figure 1 it can be seen that across the range of early-winter NAT surface areas, the chlorine reactivity due to NAT particles is much slower than the liquid aerosol reactivity. Even for occasional leewave clouds that may generate

NAT clouds with high surface areas (where reactivities could be comparable to the "NAT, New γ" values), the NAT particles are more than one order of magnitude less efficient than liquid aerosol.

Table S1: Summary of Model Simulations of Winter-Long Evolution. Five scenarios were examined, each for both one Arctic and one Antarctic winter, using a model with complete chemistry and microphysics. Averages over the vortex (both horizontally and vertically from 425 to 525 K) are shown. Chlorine activation dates were chosen to be near the peak in chlorine activation and before the effects of denitrification had significant effects. The date chosen for ozone loss in the Arctic is immediately before the vortex final warming; in the Antarctic, it is after ozone loss has maximized.

Scenario	Key Features	Vortex-Averaged Chlorine Activation (%)		Vortex-Averaged Ozone Loss (%)	
		Arctic (Feb 1st)	Antarctic (Aug 1st)	Arctic (Mar 10th)	Antarctic (Nov 1st)
FullPSC	All PSC types possible, denitrification occurs	63.4	68.1	36.3	86.9
Liquid	Liquid particles only, no denitrification	63.8	67.9	32.7	84.9
LiqBin	Binary liquid only (no STS PSCs)	63.8	68.6	32.7	83.3
LiqTACL	Temperature > T_{ACL}	50.6	50.1	26.7	50.3
LiqTACL2	Temperature > T_{ACL}-2	58.6	61.2	30.7	64.3

Table S2: Percentage of Winter-long Chlorine Activation caused by each Particle Type. Results are for the "FullPSC" scenario, integrated over all simulated air parcels for the full extent of the winter (Nov. 1st to Mar 10th in the Arctic; April 15th to Nov 1st in the Antarctic). Liquid particles were considered to be ternary solutions if more than 1 ppbv of HNO_3 was in the liquid phase, and binary otherwise.

	Arctic	**Antarctic**
Binary liquid	86.0	58.4
Ternary liquid (Type 1b PSC)	11.8	34.4
NAT (Type 1a PSC)	2.2	6.5
Ice (Type II PSC)	0.00004	0.6

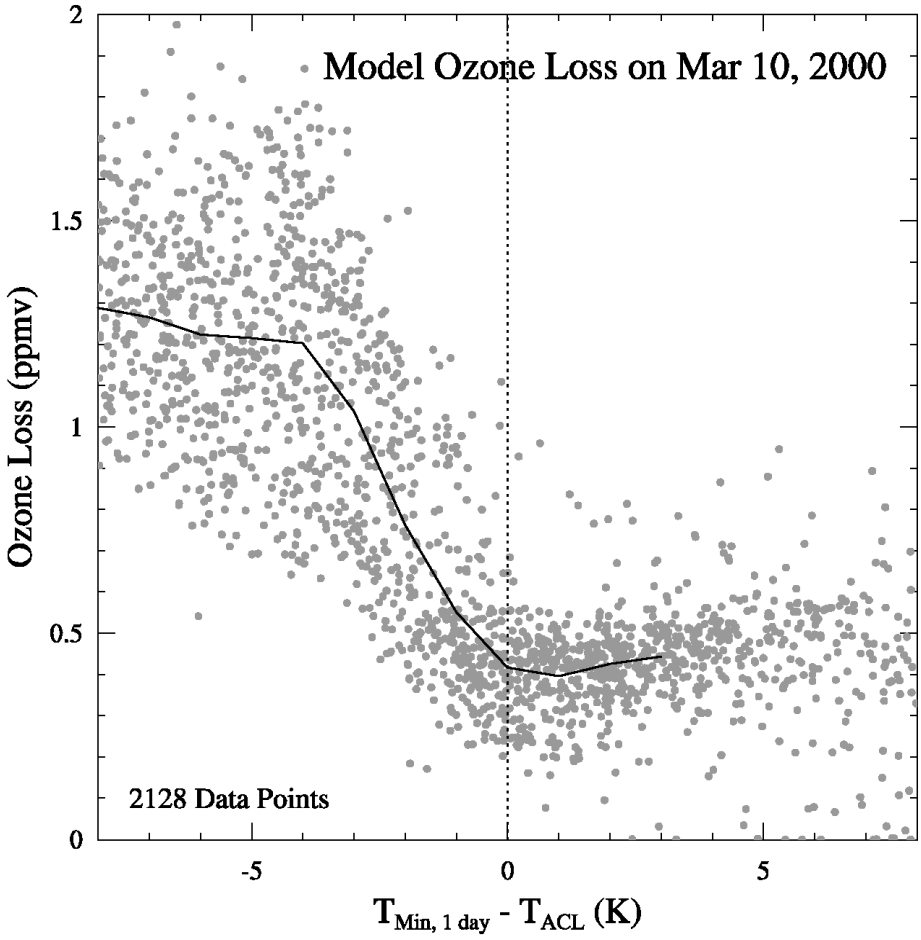

Figure S1: Ozone loss as a function of the minimum temperature (relative to T_{ACL}) to which the air had been exposed for one day. Results are shown for the Arctic "FullPSC" scenario. Ozone loss is the total chemical loss from Nov 1st to Mar 10th. Each point represents one simulated air parcel; all 2128 air parcels from 400 to 600 K are shown. The solid line is the average ozone loss in each 1 K temperature bin.

References

1 D. Hanson, K. Mauersberger, *Geophys. Res. Lett.* **15**, 855 (1988).

2 J.J. Bauman, P.B. Russell, M.A. Geller, P. Hamill, *J. Geophys. Res.* **108**, 10.1029/2002JD002993 (2003).

3 S.P. Sander *et al.*, *Chemical Kinetics and Photochemical Data for Use in Atmospheric Studies, Evaluation Number 15*, JPL Publ. 06-02 (2006).

4 K.S. Carslaw, Th. Peter, *Geophys. Res. Lett.* **24**, 1743 (1997).

5 K.S. Carslaw, B. Luo, T. Peter, *Geophys. Res. Lett.* **22**, 1877 (1995).

6 Q. Shi, J.T. Jayne, C.E. Kolb, D.R. Worsnop, P. Davidovits, *J. Geophys. Res.* **106**, 24259, 10.1029/2000JD000181 (2001).

7 M.L. Santee *et al.*, *J. Geophys. Res.* **108**, 10.1029/2002JD003335 (2003).

8 G.C. Toon *et al.*, *J. Geophys. Res.*, **104**, 26779 (1999).

9 R.W. Portmann *et al.*, *J. Geophys. Res.* **101**, 22991 (1996).

10 K. Drdla, M.R. Schoeberl, E.V. Browell, *J. Geophys. Res.*, **107**, 8312, 10.1029/2001JD000782 (2002).

11 K. Drdla, M.R. Schoeberl, *J. Geophys. Res.* **107**, 10.1029/2001JD001159 (2002).

12 C.M. Benson *et al.*, *J. Geophys. Res.* **111**, 10.1029/2005JD006506 (2006).

13 R.L. Jones *et al.*, *Geophys. Res. Lett.* **17**, 541 (1990).

14 L.R. Poole *et al.*, *Geophys. Res. Lett.* **17**, 537 (1990).

15 L. Jaeglé *et al.*, *J. Geophys. Res.* **102**, 13235 (1997).

16 J.E. Dye *et al.*, *Geophys. Res. Lett.* **17**, 413 (1990).

17 G.V. Ferry, E. Neish, M. Schultz, R.F. Pueschel, *J. Geophys. Res.* **94**, 16459 (1989).

18 J.E. Dye, B.W. Gandrud. D. Baumgardner, L. Sanford, G.V. Ferry, *Geophys. Res. Lett.* **17**, 409 (1990).

19 J.E. Dye *et al.*, *J. Geophys. Res.* **97**, 8015 (1992).

20 K. Drdla *et al.*, *Geophys. Res. Lett.* **21**, 2475 (1994).

21 K.S. Carslaw *et al.*, *Geophys. Res. Lett.* **21**, 2479 (1994).

22 A. Tabazadeh, R.P. Turco, K. Drdla, M.Z. Jacobson, O.B. Toon, *Geophys. Res. Lett.* **21**, 1619

(1994).

23 Th. Peter, *Annu. Rev. Phys. Chem.* **48**, 785 (1997).

24 C. Voigt *et al.*, *Atmos. Chem. Phys.* **5**, 1371 (2005).

25 N. Larsen *et al.*, *Atmos. Chem. Phys.* **4**, 2001 (2004).

26 M.J. Northway *et al.*, *J. Geophys. Res.* **107**, 10.l029/2001JD001079 (2002).

27 S.D. Brooks *et al., J. Geophys. Res.* **108**, 10.1029/2002JD003278 (2003).

28 A. Adriani *et al.*, *J. Geophys. Res.* **109**, 10.1029/2004JD004800 (2004).

29 A.W. Strawa *et al.*, *J. Geophys. Res.* **107**, 10.1029/2001JD000458 (2002).

30 L.R. Poole, C.R. Trepte, V.L. Harvey, G.C. Toon, R.L. Van Valkenburg, *Geophys. Res. Lett.* **30**, 10.1029/2003GL018496 (2003).

31 O.B. Toon, A. Tabazadeh, E.V. Browell, J. Jordan, *J. Geophys. Res.* **105**, 20589 (2000).

32 A. Tsias *et al.*, *J. Geophys. Res.* **104**, 23961 (1999).

33 R.-M. Hu *et al.*, *J. Geophys. Res.* **107**, 10.1029/2001JD001125 (2002).

34 C. Voigt *et al.*, *Science* **290**, 1756 (2000).